PAPER

Check for updates

Gene activated scaffolds incorporating star-shaped polypeptide-pDNA nanomedicines accelerate bone tissue regeneration *in vivo*†

David P. Walsh, [ID] [a,b,c,d] Rosanne M. Raftery, [ID] [b,c,d] Robert Murphy,[e] Gang Chen,[f] Andreas Heise, [ID] [d,e,g] Fergal J. O'Brien[a,b,c,d,g] and Sally-Ann Cryan [ID] *[a,b,c,g]

Increasingly, tissue engineering strategies such as the use of biomaterial scaffolds augmented with specific biological cues are being investigated to accelerate the regenerative process. For example, significant clinical challenges still exist in efficiently healing large bone defects which are above a critical size. Herein, we describe a cell-free, biocompatible and bioresorbable scaffold incorporating a novel star-polypeptide biomaterial as a gene vector. This gene-loaded scaffold can accelerate bone tissue repair *in vivo* in comparison to a scaffold alone at just four weeks post implantation in a critical sized bone defect. This is achieved *via* the *in situ* transfection of autologous host cells which migrate into the implanted collagen-based scaffold *via* gene-loaded, star-shaped poly(ʟ-lysine) polypeptides (star-PLLs). *In vitro*, we demonstrate that star-PLL nanomaterials designed with 64 short poly(ʟ-lysine) arms can be used to functionalise a range of collagen based scaffolds with a dual therapeutic cargo (pDual) of the bone-morphogenetic protein-2 plasmid (pBMP-2) and vascular endothelial growth factor plasmid (pVEGF). The versatility of this polymeric vector is highlighted in its ability to transfect Mesenchymal Stem Cells (MSCs) with both osteogenic and angiogenic transgenes in a 3D environment from a range of scaffolds with various macromolecular compositions. *In vivo*, we demonstrate that a bone-mimetic, collagen-hydroxyapatite scaffold functionalized with star-PLLs containing either 32- or 64- poly(ʟ-lysine) arms can be used to successfully deliver this pDual cargo to autologous host cells. At the very early timepoint of just 4 weeks, we demonstrate the 64-star-PLL-pDual functionalised scaffold as a particularly efficient platform to accelerate bone tissue regeneration, with a 6-fold increase in new bone formation compared to a scaffold alone. Overall, this article describes for the first time the incorporation of novel star-polypeptide biomaterials carrying two therapeutic genes into a cell free scaffold which supports accelerated bone tissue formation *in vivo*.

[a]*Drug Delivery & Advanced Materials Team, School of Pharmacy & Biomolecular Sciences, RCSI, Dublin, Ireland*
[b]*Tissue Engineering Research Group, Department of Anatomy & Regenerative Medicine, RCSI, Dublin, Ireland*
[c]*Trinity Centre for Biomedical Engineering, Trinity College Dublin (TCD), Dublin, Ireland*
[d]*SFI Advanced Materials and Bioengineering Research (AMBER) Centre, RCSI & TCD, Ireland*
[e]*Department of Chemistry, RCSI, Dublin, Ireland*
[f]*Centre for the Study of Neurological Disorders, Microsurgical Research and Training Facility (MRTF), RCSI, Dublin, Ireland*
[g]*SFI Centre for Research in Medical Devices (CURAM), RCSI, Dublin and National University of Ireland, Galway, Ireland*
†Electronic supplementary information (ESI) available. See DOI: 10.1039/d1bm00094b

Introduction

The field of tissue engineering (TE) has evolved in recent years from the use of biomimetic scaffolds which guide the regenerative process to advanced biotherapeutic-loaded matrices which augment and accelerate tissue repair. These constructs are designed to fill the tissue defect site and provide a physical substrate for tissue growth. They can also act as a matrix for the controlled delivery of a therapeutic, often to induce autologous host cells to proliferate and differentiate. Within our laboratory, a series of collagen based scaffolds have previously been developed to function as 3D templates for the regeneration of a range of tissues including collagen-chondroitin sulphate (collagen-CS),[2] collagen-hyaluronic acid (HyA),[3] collagen hydroxyapatite (collagen-HA)[4] and collagen-nanohydroxyapatite (collagen-nHA)[5] scaffolds. We have demonstrated the

regenerative capacity of a number of these scaffolds *in vivo* for the healing of both small animal[6] and large animal[7,8] bone defects.

Commonly, bioactive therapeutics such as small molecule drugs or growth factors are incorporated into these scaffolds to augment their regenerative capacity.[9–11] This is particularly evident in the field of bone tissue regeneration, a tissue which traditionally represents a significant challenge to efficiently heal in modern orthopedics.[12] Of these growth factors, BMP-2 is considered to be the most potent osteoinductive factor due to its ability to promote *in vitro* bone repair[13] as well as being effective in the treatment of pre-clinical human fractures.[14,15] VEGF is commonly used to encourage the direct formation of blood vessels within the scaffold as it is traditionally associated with an angiogenic action.[16] Furthermore, VEGF is known to play a key role in osteogenesis *via* a direct action on osteoblasts[15,17] as well as having a pivotal role in fracture repair.[15] Indeed, it is now established that for the successful recapitulation of bone *in vivo*, the presentation of multiple growth factors at the defect site is likely to result in enhanced functional tissue regeneration.[18] While a large number of growth factors co-operate during the bone formation process, the co-application of BMP-2 (pro-osteogenic) and VEGF (pro-angiogenic) growth factors has been shown to possess a potent, synergistic effect in mimicking the angiogenic–osteogenic coupling necessary for the formation of vascularized bone.[19–22]

While the dual delivery of therapeutic proteins to a tissue defect on scaffold based constructs is promising, it remains hindered by the repeated, supraphysiological doses of proteins required which can often result in the formation of ectopic tissue.[23] As a result, there is increasing interest in the design of gene-activated scaffolds, advanced implantable platforms which are capable of delivering gene therapeutics in a controlled and localized manner at the defect site.[24,25] This promising combination of gene therapy and TE relies on the use of vectors which are capable of transfecting autologous host cells to induce *in vivo* protein expression. This *in vivo* expression provides a physiologically relevant protein dose which is localized at the defect site.

A critical aspect to the translation of gene-activated scaffolds is a biocompatible and efficient vector which is capable of efficiently transfecting infiltrating autologous host cells *in vivo* within the 3D matrix. A number of concerns associated with the use of viral based vectors, such as prolonged and expensive manufacturing costs, the risk of toxicity, immunogenicity and insertional mutagenesis has focused the field on the design of synthetic, bioinspired non-viral vector systems.[24] Since the seminal works on gene activated scaffolds,[26,27] numerous non-viral gene delivery vectors have been evaluated for TE.[24] Despite the multitude of potential non-viral vector candidates, few have been successfully translated *in vivo* due to underlying limitations with the vector themselves such as toxicity[28] or poor transfection efficiency.[29]

Star-polypeptides are a broad class of branched polymeric architectures which consist of linear polypeptide arms radiat-

ing from a central core.[30] Previously, we have extensively described a novel class of bioinspired star-shaped poly(L-lysine) polypeptides with varying number and length of attached poly(L-lysine) arms referred to as star-PLLs. We have demonstrated that star-PLLs are capable of rapidly self-assembling with plasmid DNA (pDNA) to form a nanomedicine. These nanomedicines can facilitate non-toxic, efficient transfection of mesenchymal stem/stromal cells (MSCs) with subsequent bioactive, therapeutic protein expression.[31] Intracellular delivery of the star-PLL-pDNA complex to MSCs is achieved *via* a claritin independent internalization process.[31] Furthermore, we have highlighted the capacity of star-PLLs to effectively functionalize a range of collagen based scaffolds *in vitro* and function as a biocompatible nanomedicine depot for reporter genes *in vivo*.[1] These star-PLL functionalized scaffolds were capable of facilitating autologous host cell transfection at the early timepoint of just 7 days post implantation.[1]

Building upon our previous work, this study aimed to create for the first time a therapeutically active, cell-free, gene activated scaffold which is specifically tailored for the rapid regeneration of bone tissue using the star-PLL nanomaterials. Two star-PLL compositions were evaluated during this study which encompassed structural variations to the polypropylene imine (PPI) dendrimer core generation (4th generation or 5th generation), the poly(L-lysine) arm number (32 arms or 64 arms) and the number of poly(L-lysine) subunits per arm number (40 subunits or 5 subunits) namely; $G4(32)PLL_{40}$ (32-star-PLL) & $G5(64)PLL_5$ (64-star-PLL). Initially, we optimized the star-PLL-pDNA gene activated scaffold platform for the osteogenic differentiation of MSCs *in vitro* by varying the gene cargo delivered and the macromolecular composition of the scaffold used. Following identification of a lead platform for bone tissue repair we assessed the translational potential of these optimized star-PLL-pDNA gene activated scaffolds *in vivo*. In these studies their ability to accelerate the healing of a critical sized rodent (rat) calvarial bone defect *in vivo* at an early timepoint of 4-weeks post implantation was evaluated.

Materials and methods

All materials were supplied by Sigma-Aldrich, Ireland unless otherwise stated.

Plasmid propagation & purification

The therapeutic plasmids Bone Morphogenetic Protein-2 (pBMP-2), kindly donated by Prof. Kazihusa Bessho, Kyoto University, Japan and Vascular Endothelial Growth Factor (pVEGF, Genecopaeia, USA) were propagated *via* the transformation of Subcloning Efficiency™ DH5α™ chemically competent *Escherichia coli* cells (Life Technologies, Ireland). Both plasmids were isolated and purified using an Endotoxin Free Maxi-prep Kit (Qiagen, UK) as per the manufacturer's instructions.

Mesenchymal stem cell culture

Rat mesenchymal stem/stromal cells (MSCs) were purchased from C&M LabPro (Pittsburgh, USA). Cells were obtained at a passage 1 and cultured at a seeding density of 1×10^6 cells per T175 flask until they reached 80–90% confluency. MSCs were cultured in two different media. Growth medium (GM) consisted of Dulbecco's modified Eagle's medium (DMEM) supplemented with: 2% penicillin/streptomycin, 1% glutamax, 1% L-glutamine, 1% non-essential amino acids and 10% FBS while osteogenic medium (OM) consisted of DMEM supplemented with 10% FBS, 1% penicillin/streptomycin, 10 mM β-glycerophosphate, 50 μM ascorbic acid 2-phosphate and 100 nM dexamethasone. Cells were maintained under standard cell culture conditions during all experiments (37 °C, 5% CO_2, 90% humidity) and all *in vitro* experiments were carried out using passage 5 cells.

Star-shaped poly(L-lysine) polypeptide synthesis

Star-PLLs were synthesized as previously described *via* an *N*-carboxyanhydride ring opening polymerization reaction.[32] Two star-PLL polymeric architectures were used to form the gene-activated scaffolds described in this study namely; 32-star-PLL and 64-star-PLL. The structural composition of both star-PLLs have been previously described by our group[1] and are outlined below in Fig. 1.

Preparation of star-PLL-pDNA nanomedicines

All nanomedicines were formulated at an N/P 5 (the molar ratio of positively charged nitrogen arms present in the star-PLL to negatively charged phosphate groups present in the pDNA molecule) and a total pDNA dose of 5 μg. This formu-

lation has previously been optimized by our group for the transfection of MSCs in a 3D matrix.[1] Star-PLL-pDNA nanomedicines were formed containing either of pBMP-2, pVEGF or a dual combination of pBMP-2 and pVEGF (pDual). The pDual formulation contained a 50 : 50 mix of pBMP-2 and pVEGF *i.e.* 2.5 μg pBMP-2 and 2.5 μg pVEGF to give a total 5 μg pDNA dose. Briefly, nanomedicines were formed *via* the dropwise addition of star-PLL polymeric material to pDNA in molecular biology grade H_2O. Complexation was allowed to proceed for approximately 5–10 minutes at room temperature prior to use.

Gene-activated scaffold fabrication

Five different bovine collagen (Southern Lights Biomaterials, New Zealand) based scaffolds were used in this study; collagen alone, collagen-CS, collagen-HyA, collagen-HA and collagen-nHA scaffolds. For all scaffold variants, collagen or collagen composite slurries were lyophilized using an optimized protocol.[3–5,33] The specific formation of each of these scaffolds has been previously detailed by us elsewhere.[34,35] Scaffolds were cross-linked dehydrothermally (DHT) at 105 °C for 24 hours in a vacuum oven (Vacucell 22; MMM, Germany) and subsequently cut into cylindrical 9.6 mm sections for *in vitro* experiments. For *in vivo* experiments, scaffolds were fabricated with an 8 mm diameter to fit the calvarial defect.

Prior to use, each scaffold was rehydrated in 2 mL of PBS and then chemically cross-linked using a mixture of 14 mM *N*-(3-dimethylaminopropyl)-*N*′-ethylcarbodiimide hydrochloride (EDC) and 5.5 mM *N*-hydroxysuccinimide (NHS).[36] To form a functional gene activated scaffold, nanomedicines were formed as previously described in either a 50 μL (*in vitro* experiments) or 30 μL (*in vivo* experiments) final volume. For
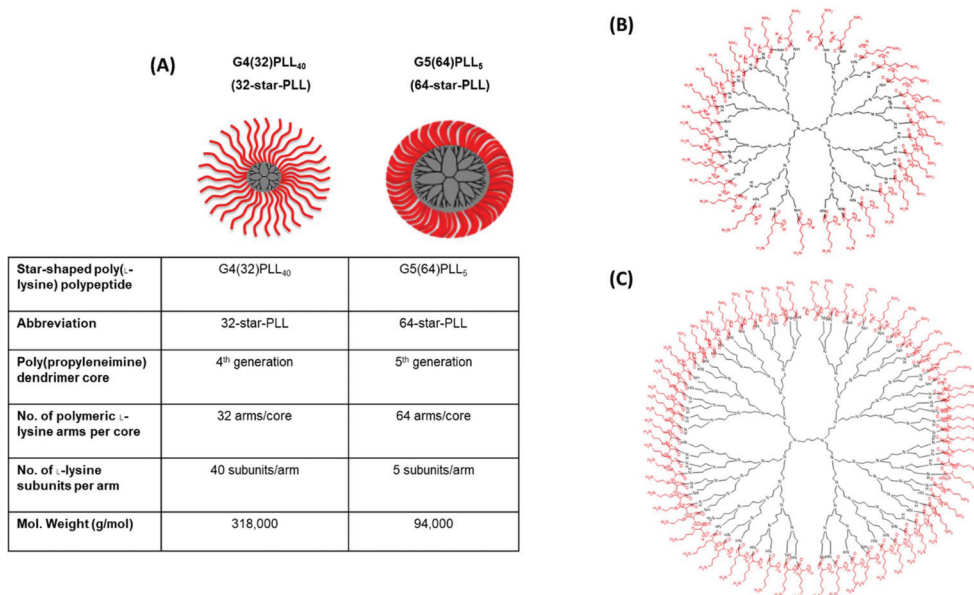

Star-shaped poly(L-lysine) polypeptide	G4(32)PLL₄₀	G5(64)PLL₅
Abbreviation	32-star-PLL	64-star-PLL
Poly(propyleneimine) dendrimer core	4th generation	5th generation
No. of polymeric L-lysine arms per core	32 arms/core	64 arms/core
No. of L-lysine subunits per arm	40 subunits/arm	5 subunits/arm
Mol. Weight (g/mol)	318,000	94,000

Fig. 1 Structural overview of star-PLLs. Illustrated above is (A) a structural outline of the two star-PLLs used in this study, namely G4(32)PLL₄₀ (32-star-PLL) and G5(64)PLL₅ (64-star-PLL), (B) chemical structure of 32-star-PLL and (C) chemical structure of 64-star-PLL. Reproduced from ref. 1 with permission from Elsevier, copyright 2018.

in vitro experiments, each scaffold was placed into a well of a 24 well suspension tissue culture plate and 25 μL of nano-medicine suspension was soak loaded onto one side of the scaffold. The scaffold was incubated for 15 minutes at 37 °C and 2×10^5 MSCs were added to the same side of the scaffold in a 25 μL volume of OptiMEM. Following a further 15-minute incubation, the scaffolds were carefully inverted, and the additions and incubations repeated on the opposite side (total pDual volume per scaffold = 50 μl). For *in vivo* experiments, approximately 15 μL of nanomedicine solution was soak loaded onto each side of the scaffold prior to implantation into the defect (total pDual volume per scaffold = 30 μl).

In vitro experiments

Scaffold osteogenesis assay. Gene activated scaffolds were formed as previously described containing each of 64-star-PLL-pBMP-2 (N/P 5, 5 μg pBMP-2), 64-star-PLL-pVEGF (N/P 5, 5 μg pVEGF) or 64-star-PLL-pDual (N/P 5, 2.5 μg pBMP-2 & 2.5 μg pVEGF). MSCs were seeded onto the gene-activated scaffolds as described above. Non-gene loaded scaffolds functioned as controls for this experiment. Scaffolds were cultured in GM under standard conditions for 3 days before being transferred to a new well containing OM. At day 28 post-GM to OM change, each scaffold was removed from culture and placed into 1 mL of 0.5 M hydrochloric acid in an Eppendorf tube. Scaffolds were then rocked at 4 °C for approximately 48 hours to ensure solubilization of all calcium. Calcium content was determined using a Stanbio calcium assay (Calcium CPC Liquicolour, Stanbio Inc. USA) as per the manufacturer's instructions. Samples were prepared in 0.5 M hydrochloric acid and absorbance of the color generated was read at 595 nm using a Varioskan Flash plate reader. The concentration of calcium per scaffold was determined against a standard curve.

Scaffold DNA quantification assay. The quantification of dsDNA present in each scaffold was determined using a Quant-iT™ PicoGreen® dsDNA kit (Invitrogen, UK). Briefly, gene activated scaffolds containing each of 64-star-PLL-pBMP-2 (N/P 5, 5 μg pBMP-2), 64-star-PLL-pVEGF (N/P 5, 5 μg pVEGF) or 64-star-PLL-pDual (N/P 5, 2.5 μg pBMP-2 & 2.5 μg pVEGF) were formed as previously described and seeded with MSCs. Non-gene loaded scaffolds functioned as controls for this experiment. Scaffolds were cultured as described above in GM for 3 days followed by OM up to day 28. Each scaffold was then removed from culture and submerged in 1 mL of cell lysis buffer (0.2 M carbonate buffer containing 1% Triton-X). Scaffolds were subjected to three freeze–thaw cycles at −80 °C to ensure complete cell lysis and 100 μL of each sample was added in triplicate to a black 96 well plate. Quant-iT™ PicoGreen® reagent (100 μL) was then added to each well and the plate incubated for 3–5 minutes at room temperature. Fluorescence was determined using an excitation wavelength of 485 nm and emission wavelength of 538 nm. The concentration of dsDNA present in each sample was determined using a standard curve and each sample was corrected against a respective non-MSC seeded gene activated scaffold to control for the detection of exogenously delivered pDNA.

Alizarin red staining of scaffolds for calcium. Alizarin red staining was used to visualize the level of mineralization occurring within each of 64-star-PLL-pBMP-2, 64-star-PLL-pVEGF or 64-star-PLL-pDual gene activated scaffolds. Scaffolds were fabricated, soak loaded with nanomedicines and seeded with MSCs as described above. At day 28 post-seeding scaffolds were transferred to 1 mL of 10% formalin for 1 hour at room temperature. Samples were then processed overnight using an automatic tissue processor (ASP300, Leica, Germany). Each sample was then embedded in paraffin wax before 7 μm sections were cut using a rotary microtome (Microsystems GmbH, Germany). Sections were mounted onto poly(ʟ-lysine) coated glass slides and dried in an oven overnight at 60 °C. Each section was then deparaffinised with xylene, rehydrated in descending grades of alcohol and stained in 2% alizarin red stain (pH 4.2) for 5 minutes. Sections were then dehydrated in ascending grades of alcohol, cleared in xylene and coverslips mounted using DPX mountant. Images were captured using a transmitted light microscope (Nikon Microscope Eclipse 90i with NIS elements software v3.06) (Nikon instruments, Holland). Calcium is visible as red deposits.

In vivo experiments

Calvarial defect surgical procedure. To assess the ability of gene activated scaffolds to promote bone tissue regeneration, a 7 mm critical sized calvarial defect model was used in young adult male, Wistar rats (weight range 300–340 g) (Envigo, UK). All animal procedures were performed in accordance with the Guidelines for Care and Use of Laboratory Animals of the Royal College of Surgeons in Ireland and approved by the Research Ethics Committee of the Royal College of Surgeons in Ireland (REC Approval #1350). Additionally, an animal project license was granted by the Irish Health Products Regulatory Authority (Authorization # AE19127/P036) in compliance with EU directive 2010/EU/63. This animal model is used in 38% of all critical calvarial defect studies for bone regeneration[37,38] and is well established within our laboratory and described in detail elsewhere by our group.[6,22,29,39–41] A total of 40 male Wistar rats were divided into five treatment groups (*n* = 8 animals per group), each of which is described below in Table 1. Once fabricated, each scaffold was implanted into the defect and the periosteum was sutured using Vicryl® 3-0 absorbable sutures (Ethicon, USA). The wound was then further secured using a topical skin adhesive (*n*-butyl cyanoacrylate) (Vetbond™). Animals were housed with free access to food and water during the study. Antibiotic prophylaxis was administered in the drinking water in the form of Baytril® (enrofloxacin) (5 mg kg^{-1}) for 3 days post-surgery. At four weeks post-implantation the animals were euthanized by CO_2 asphyxiation followed by cervical dislocation. A 20 mm × 20 mm segment of calvarium containing the defect site was resected using a dental saw (Osung Dental, USA). The explants were washed in PBS until clear washout was observable before fixation in 10% formalin for 72 hours at 4 °C. Explants were then stored in PBS at 4 °C prior to analysis.

Table 1 Summary of experimental groups used in the calvarial defect study

Treatment group	Number of animals	N/P ratio	pDNA dose	Abbreviation
Gene-free collagen-HA	8	—	—	Gene-free scaffold
G4(32)PLL$_{40}$-pDual collagen-HA	8	N/P 5	2.5 µg pBMP-2 & 2.5 µg pVEGF	32-star-PLL-pDual scaffold
G4(32)PLL$_{40}$-(no gene) collagen-HA	8	—	—	32-star-PLL-(no gene) scaffold
G5(64)PLL$_5$-pDual collagen-HA	8	N/P 5	2.5 µg pBMP-2 & 2.5 µg pVEGF	64-star-PLL-pDual scaffold
G5(64)PLL$_5$-(no gene) collagen-HA	8	—	—	64-star-PLL-(no gene) scaffold

A total of 40 male Wistar rats were used for this study with 8 animals per treatment group. Groups assessed included a collagen-HA scaffold alone or a collagen-HA scaffold soak loaded with 32-star-PLL-pDual, 32-star-PLL-(no gene), 64-star-PLL-pDual or 64-star-PLL-(no gene). Both star-PLL-(no gene) formulations contained the same µg dose of star-PLL as would be present in the pDual complexed formulation but did not contain pDNA.

Assessment of new bone formation within the calvarial defect. MicroCT analysis was used to both qualitatively and quantitatively assess new bone formation within each defect. A 20 mm × 20 mm section of calvaria was excised at four weeks. Scans were performed on a Scanco Medical 40 MicroCT system (Scanco Medical, Switzerland) with a voxel resolution of 12 µm, a 70 kVP X-ray source and 112 µA current. A reconstructed 3D tomogram was formed using the Scanco software package which consisted of 300 sliced, 2D projection images (a threshold of 140, scale from 0 to 1000, density of 257.99 mg HA per cm). These settings have been optimized for the rat calvarial model previously and are routinely used within our group.[21,22,29,40,41] Although a 7 mm defect was created during each surgical procedure, a 6 mm region of interest (ROI) was chosen for analysis to ensure only new bone within the defect was being analysed and any original host bone at the periphery was accounted for. Bone formation was expressed as a percentage new bone volume over total bone volume (BV/TV) within this ROI.

Histological assessment of calvarial defect. To corroborate the microCT analysis, both qualitative and quantitative histology was performed on excised calvaria. Each specimen was submerged in decalcifying solution-lite® for approximately 13 hours to remove all calcium. Decalcification was confirmed via an endpoint chemical test as per the manufacturer's instructions. Specimens were processed overnight using an automatic tissue processor (ASP300, Leica, Germany). Following processing, the defect was bisected using a backed blade and each specimen embedded in a paraffin block. Each block was cut using a rotary microtome (Microsystems GmbH, Germany) into 7 µm sections from the mid-section of each block, sections were mounted onto poly(L-lysine) slides and dried overnight in an oven at 60 °C. Histological assessment was performed using hematoxylin and eosin (H&E) staining and Masson's Trichrome (MT) staining. H&E staining was performed on each specimen (n = 40 animals). Each section was deparaffinised with xylene and rehydrated in descending grades of alcohol. They were then stained with filtered hematoxylin stock solution (1%) for four minutes and eosin (0.05%) for two minutes. The sections were then dehydrated through ascending grades of alcohol, cleared in xylene and coverslips were mounted using DPX mounting media. Images of each section were acquired and digitized using a transmitted light microscope (Nikon Microscope Eclipse 90i with NIS elements software v3.06) (Nikon instruments, Holland). Quantitative histomorphometry was carried out on n = 6 sections from each specimen (total specimens = 40, quantified sections = 240) to quantify the healing response from the H&E stained samples. New bone formation was quantified via measuring the area of bone nucleation sites within each section and calculating the mean total area of these sites per treatment group. The defect margins were identified using Fiji image processing software and the area of new bone was then calculated using a Fiji macro[42] (automated method of pixel saturation quantification) and expressed as the area of new bone formed (µm^2). Assessment was carried out via a single blind approach.

For Masson's Trichrome staining, 7 µm sections from each treatment group (approximately 3 animals per treatment group) were chosen at random and deparaffinised with xylene before being rehydrated in descending grades of alcohol. Slides were then allowed to mordant in Bouin's solution for approximately 1 hour at 60 °C. Each slide was then consecutively stained in Weigert's iron hematoxylin solution, Biebrich scarlet-acid fuchsin solution, phosphotungstic/phosphomolybdic acid solution and finally aniline blue solution for five minutes each. Samples were then rinsed in acid alcohol, dehydrated through ascending alcohol grades, cleared in xylene and mounted with coverslips using DPX mountant. Images were captured as previously described using a Nikon microscope.

Statistical analysis

All results are expressed as the mean ± standard deviation (SD). Statistical significance was determined using a one-way ANOVA plus Tukey post-hoc test. For in vivo results two outliers were identified using a Grubb's test and eliminated from further analysis. Values which were considered statistically significant were *$p < 0.05$, **$p < 0.01$, ***$p < 0.001$ & ****$p < 0.0001$. Data was analysed using GraphPad Prism v6.1 software.

Results

Combinatorial delivery of pBMP-2 and pVEGF using star-polypeptides facilitates enhanced *in vitro* MSC mediated osteogenesis on collagen based scaffolds

Recently, we have demonstrated that star-polypeptide loaded gene activated scaffolds are capable of efficiently transfecting

MSCs from a range of collagen scaffolds both *in vitro* and *in vivo* using both reporter genes (green fluorescence protein pDNA or luciferase pDNA) and therapeutic transgenes (pBMP-2 or pVEGF).[1] It is now established that the dual application of BMP-2 and VEGF proteins can enhance the osteogenic potential of MSCs within an *in vivo* environment *via* a synergistic osteogenic–angiogenic coupling effect.[20,29] To assess if this finding translated to gene delivery using the previously identified lead star-PLL vector, 64-star-PLL,[1,31] a series of collagen-CS gene activated scaffolds loaded with 64-star-PLL-pBMP-2, 64-star-PLL-pVEGF or 64-star-PLL-pDual were assessed for their osteogenic potential *in vitro* (Fig. 2). Collagen-CS scaffolds incubated in growth media (GM) or osteogenic media (OM) were used as controls.

The highest level of calcium deposition was facilitated using the 64-star-PLL-pDual collagen-CS scaffold with 577.8 ± 6.3 μg per scaffold deposited at day 28 (Fig. 2A). This was statistically higher than that of the OM scaffold alone which caused deposition of 433.6 ± 13.5 μg per scaffold ($p < 0.05$). While a trend existed towards enhanced calcium deposition using both the 64-star-PLL-pVEGF (549.7 ± 47.8 μg per scaffold) and 64-star-PLL-pBMP-2 (527.4 ± 88.9 μg per scaffold) scaffolds, these results were not significantly increased over the OM scaffold or compared to one another. As a surrogate marker of MSC proliferation, the dsDNA present in each scaffold at 28 days was quantified, correcting for the exogenously delivered pDNA dose. A reduction in the quantity of

dsDNA present per scaffold was recorded for all treatment groups including the OM group when compared to the GM control. This failed to reach significance indicating that the gene activated constructs were not adversely affecting MSC proliferation (Fig. 2B). Alizarin red staining was used as a visual marker of calcium deposition (Fig. 2C). Staining revealed enhanced deposition of calcium (red deposits) for all gene activated scaffold treatment groups and the OM scaffold. Minimal calcium deposition was observed for the GM control group.

Effect of collagen scaffold composition on star-PLL-pDual mediated osteogenesis

In this study we sought to determine the effect of scaffold macromolecular composition on the ability of 64-star-PLL-pDual formulations to enhance MSC osteogenesis to determine the optimal therapeutic star-PLL-scaffold system for bone TE (Fig. 3). Collagen scaffolds assessed included collagen alone, collagen-HyA, collagen-nHA and collagen-HA. The 64-star-PLL-(no gene) scaffold group and each respective scaffold alone, all in OM, were used as controls. Scaffolds containing ceramic (collagen-HA and collagen-nHA) resulted in a higher level of calcium deposition compared to scaffolds containing glycosaminoglycans (collagen-CS and collagen-HyA). The highest level of calcium deposition was recorded for the 64-star-PLL-pDual collagen-HA scaffold at 28 days (2362.7 ± 164.8 μg per scaffold) (Fig. 3(A)(iv)). This was significantly increased ($p < 0.05$) compared with the corresponding col-
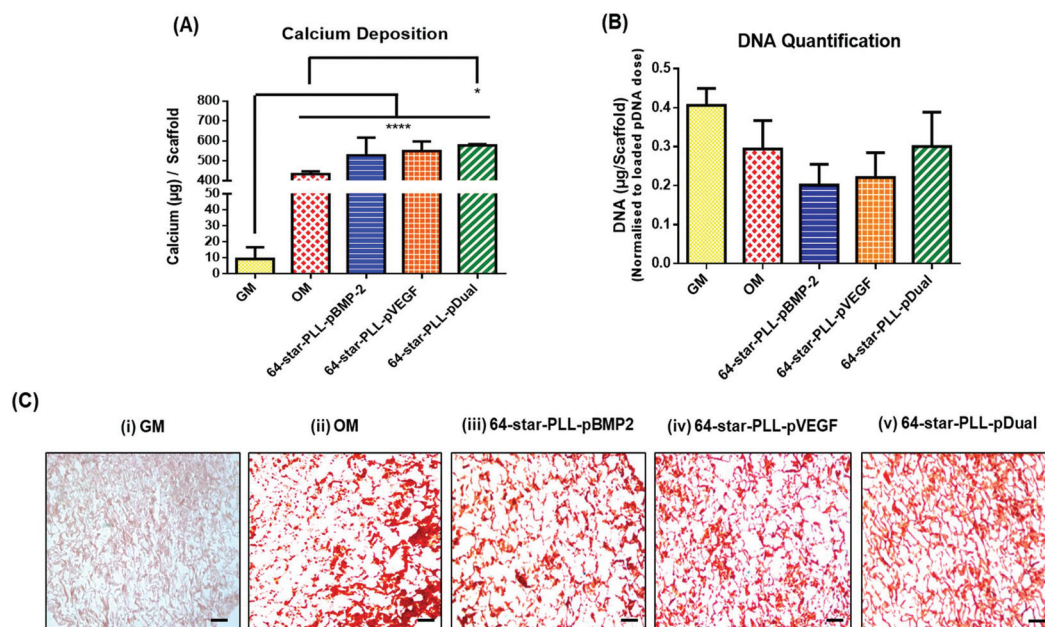

Fig. 2 A dual therapeutic cargo of pBMP-2 and pVEGF delivered using 64-star-PLL facilitates enhanced *in vitro* MSC mediated osteogenesis within a collagen-CS scaffold. (A) Calcium deposition was assessed following seeding of MSCs onto a collagen-CS scaffold with either 64-star-PLL-pBMP-2 (N/P 5, 5 μg pBMP-2), 64-star-PLL-pVEGF (N/P 5, 5 μg pVEGF) or 64-star-PLL-pDual (N/P 5, 5 μg pDual). The 64-star-PLL-pDual gene activated scaffold exhibited the highest level of calcium deposition 28 days post seeding with MSCs ($n = 3$). (B) DNA quantification revealed that a significant reduction in DNA levels per scaffold did not occur for any group ($n = 3$). (C) Representative alizarin red stains from sections of each scaffold group with positive calcium deposition observed as a red deposit. Staining was evident for all groups except the scaffold incubated in (i) GM. GM = scaffold alone in growth medium, OM = scaffold alone in osteogenic medium. Scale bar = 200 μm. Results are expressed as the mean ± SD where *$p < 0.05$ & ****$p < 0.0001$.
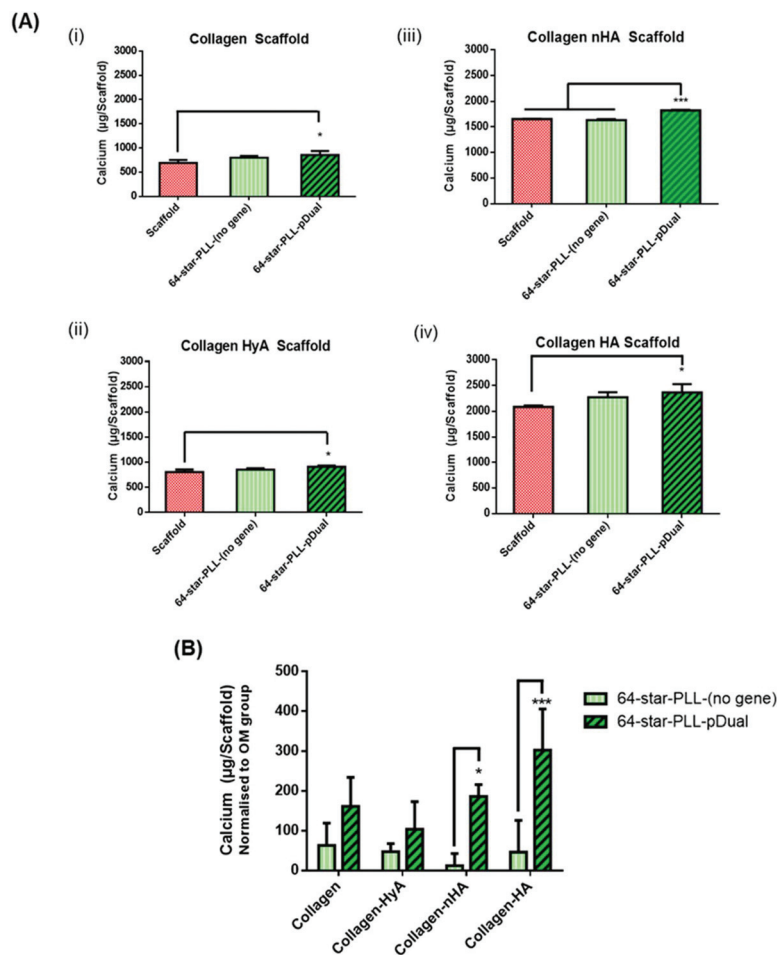
Fig. 3 Maximal MSC mediated osteogenesis is facilitated by a star-PLL-pDual collagen-HA scaffold. (A) Illustrated above is calcium deposition by MSCs quantified 28 days post seeding on each of a 64-star-PLL-pDual (5 µg pDual dose) on (i) collagen, (ii) collagen-HyA, (iii) collagen-nHA and (iv) collagen-HA scaffolds. Overall, higher levels of calcium deposition were observed for ceramic based scaffolds (collagen-nHA & collagen-HA) over non-ceramic scaffolds (collagen & collagen-HyA). Increased levels of calcium deposition was evident for all 64-star-PLL-pDual loaded scaffolds compared to a respective control scaffold alone. (B) The calcium levels deposited were then normalized to the effects of an OM control scaffold. These results highlight the collagen-HA scaffold, functionalized with the 64-star-PLL-pDual formulation as optimal in facilitating osteogenesis in MSCs. Data is expressed as the mean $\pm$ SD ($n = 3$) where *<0.05 & ***<0.001.

lagen-HA scaffold (2080.7 ± 28.9 µg per scaffold). The 64-star-PLL-(no gene) scaffold group resulted in a trend towards increased calcium deposition compared to each of its corresponding scaffolds alone, however this failed to reach significance in any of the scaffolds assessed (Fig. 3(A)(i–iv)). Notably, this effect was related to the complete star-polypeptide structure, as no significant increase in calcium deposition by MSCs was observed when the star-PLL structural components *i.e.* linear poly(L-lysine) or a poly(propyleneimine) dendrimer were used separately to treat MSCs (ESI Fig. 1†).

When normalized to the effects of the osteogenic media (*i.e.* the amount of calcium deposited by a scaffold alone) we can determine the effect of both the 64-star-PLL vector alone without a gene cargo and the 64-star-PLL-pDual formulation (Fig. 3 (B)). Here, a benefit of the pDual gene cargo is evident in both the collagen-nHA ($p < 0.05$) and collagen-HA ($p < 0.001$) scaffolds where statistically significant increases in

calcium were seen compared to scaffolds loaded with the 64-star-PLL-(no gene) formulation. By varying the amount of 64-star-PLL used at a constant pDual dose (5 µg) we further confirmed calcium deposition is primarily mediated by this pDual cargo (ESI Fig. 2†). Overall, these results highlight the collagen-HA scaffold as the collagen scaffold of choice for induction of maximal MSC mediated osteogenesis.

Gene activated scaffolds incorporating star-PLL-pDual nanomedicines accelerate bone tissue regeneration *in vivo*

A critical sized calvarial defect was used to interrogate the translational potential of the star-PLL-pDual loaded collagen-HA scaffold to facilitate bone tissue regeneration at the early time point of 4 weeks. To control for the potential effect of the star-PLL structure *in vivo*, two structural variants, namely 32-star-PLL and 64-star-PLL were assessed. The pDual cargo used *in vivo* was the same as that used *in vitro i.e.* a

50 : 50 mixture of pBMP-2 and pVEGF. The groups assessed are outlined in Table 1 and included both scaffold alone and star-PLL-(no gene) scaffold (both 32-star-PLL & 64-star-PLL) control groups as well as the 32-star-PLL-pDual scaffold and 64-star-PLL-pDual scaffold treatment groups. Qualitative assessment of the 3D reconstructions of excised calvarium (Fig. 4A) indicated that the highest level of new bone tissue formation was observed for the 64-star-PLL-pDual scaffold (Fig. 4A(v)) compared to all other scaffolds assessed. The 32-star-PLL-pDual scaffold (Fig. 4A(iii)) resulted in an increased amount of bone regeneration compared to the scaffold alone group. Finally, both star-PLL gene-free scaffolds (32-star-PLL-(no gene), Fig. 4A(ii) & (64-star-PLL-(no gene), Fig. 4A(iv)) appeared to result in enhanced bone regeneration compared to the scaffold alone.

Quantitative assessment of a 6 mm region of interest (ROI) was selected to quantify the healing response (% new bone volume) (Fig. 4B). These results corroborate the qualitative data with the 64-star-PLL-pDual scaffold resulting in the highest BV/TV % of 13.2 ± 3.4%. This scaffold induced a significant increase in new bone volume compared to the 64-star-PLL-(no gene) scaffold (5.5 ± 4.3%) ($p < 0.05$), the 32-star-PLL-(no gene) scaffold (3.3 ± 0.8%) ($p < 0.001$) and the scaffold alone (2.1 ± 0.9%) ($p < 0.0001$). The 32-star-PLL-pDual scaffold (9.4 ± 7.4%) also induced a significant increase in new bone volume compared to the scaffold alone ($p < 0.05$). Both the 32-star-PLL-(no gene) scaffold and 64-star-PLL-(no gene) scaffold showed a trend of increased new bone volume compared to the scaffold alone, however these findings were not significantly different to the scaffold alone.

Gene activated scaffolds incorporating star-PLL-pDual nanomedicines result in the formation of mineralised bone *in vivo*

Histological assessment of each defect was performed to further characterize the bone healing response for each gene-activated scaffold (Fig. 5). H&E stains cell nuclei purple, ECM pink and bone dark pink/red and was used to quantify the
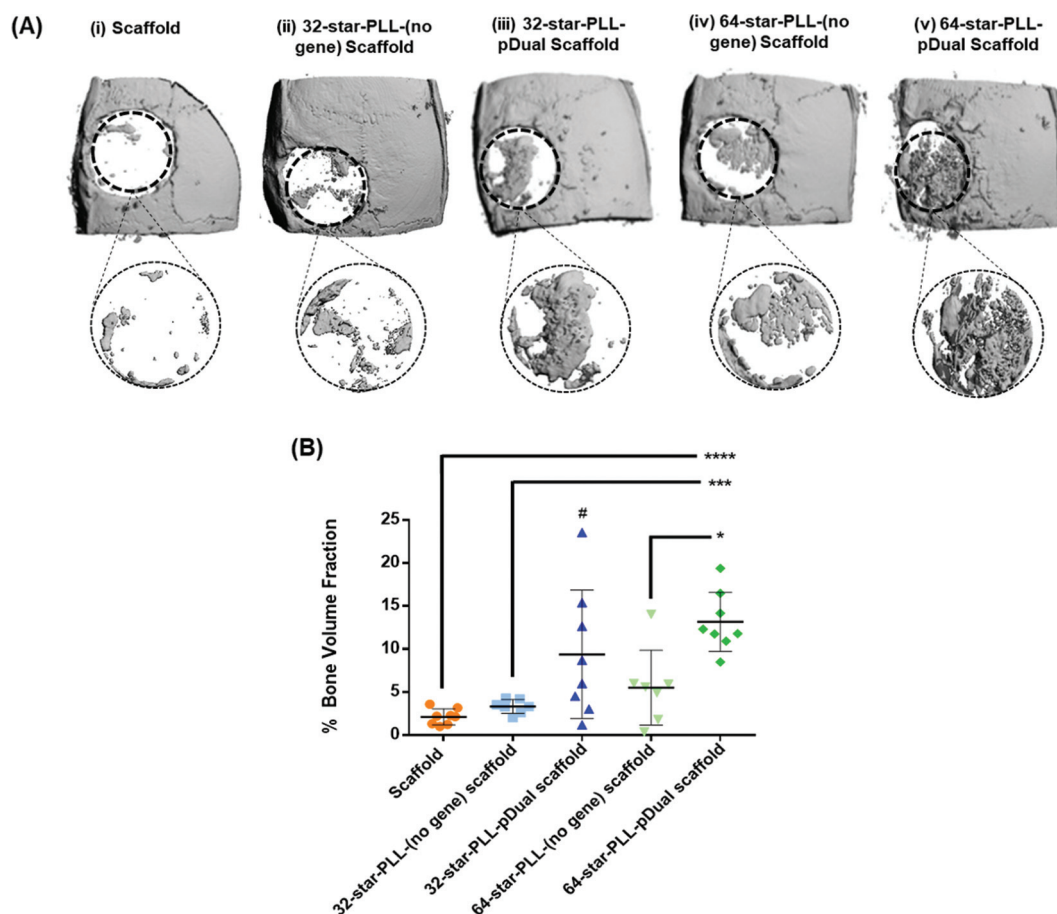

Fig. 4 Star–PLL–pDual collagen-HA scaffolds accelerate bone tissue regeneration *in vivo*. Four weeks post implantation of gene activated collagen-HA scaffolds into a critical bone defect in male Wistar rats, defects were excised and assessed using microCT. (A) A 6 mm ROI was selected for quantitative analysis of each treatment group; (i) scaffold, (ii) 32-star-PLL-(no gene) scaffold, (iii) 32-star-PLL-pDual scaffold, (iv) 64-star-PLL-(no gene) scaffold and (v) 64-star-PLL-pDual scaffold. (B) Quantitatively, both the 32-star-PLL-pDual scaffold & the 64-star-PLL-pDual scaffold resulted in enhanced new bone volume compared to the scaffold alone group. Outliers have been removed from the analysis using a GRUBBs test. Results are expressed as the mean ± SD where ****$p < 0.0001$, ***$p < 0.001$ & *$p < 0.05$. # represents statistical significance of $p < 0.05$ between the gene free scaffold group (orange) and the 32-star-PLL-pDual scaffold group (dark blue).
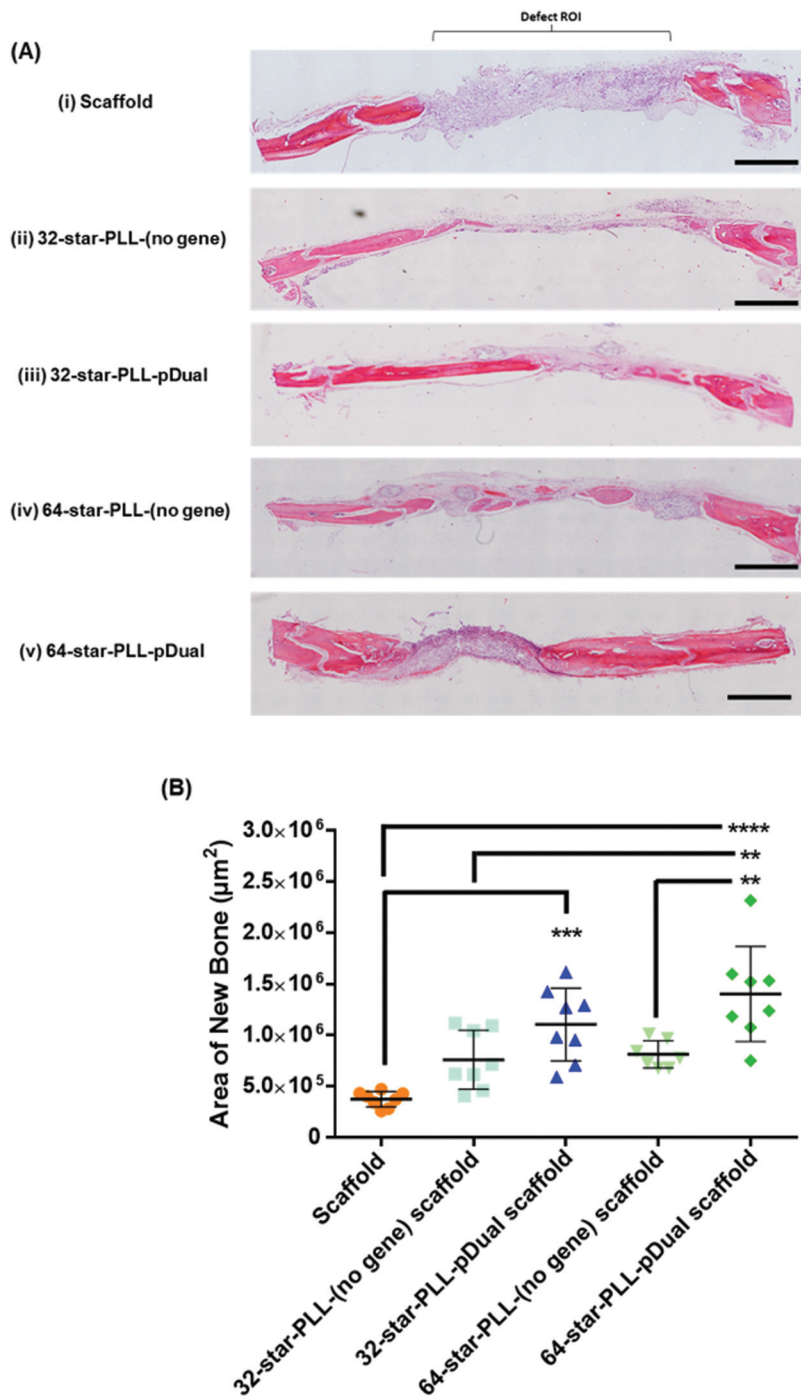
Fig. 5 Star-PLL-pDual collagen-HA scaffolds accelerate the deposition of mineralised osteoid. Four weeks post implantation of gene activated collagen-HA scaffolds into a critical bone defect in male Wistar rats, defects were excised and assessed histologically. (A) Representative H&E stained sections through the centre of each critical defect demonstrating the degree of bone healing at 4 weeks for each treatment scaffold (i–v). The highest levels of bone healing were observed for the 64-star-PLL-pDual scaffold (A (v)). (B) Quantification of the area of new bone formation using histomorphometrical analysis corroborated these results. Outliers have been removed from the analysis using a GRUBBs test. Results are expressed as the mean area of new bone detected within the defect (μm²) ± SD where ****$p < 0.0001$, ***$p < 0.001$, **$p < 0.01$. Scale bar = 1000 μm.

area of new bone formation and visualize the extent of cellular influx to the scaffold. Qualitatively, within the scaffold alone group (Fig. 5A(i)), the scaffold itself was visually evident, containing highly cellularised areas towards the peripheries of the

defect with minimal new bone detected. At this early timepoint of 4 weeks, clear boundaries between the scaffold alone and host tissue were visible. The 64-star-PLL-pDual scaffold (Fig. 5A(v)) demonstrated the most advanced healing whereby

partial bridging of the defect was evident in some specimens. Furthermore, this scaffold resulted in large areas of deeply stained bone nucleation sites, brightly stained osteoid and the scaffold appeared well integrated with the host (Fig. 5A(v)). Staining of the 32-star-PLL-pDual scaffold (Fig. 5A(iii)) revealed areas of brightly stained new bone within the defect and more advanced healing compared to the scaffold alone group. Both the 32-star-PLL-(no gene) scaffold (Fig. 5A(ii)) and the 64-star-PLL-(no gene) scaffold (Fig. 5A(iv)) groups contained areas of brightly stained new osteoid and pockets of new bone formation. In both instances, each defect was highly cellularised and healing appeared more advanced than the scaffold alone group. Overall, a clear increase in new bone formation was evident when a pDual cargo was delivered with either vector relative to the comparative scaffold alone.

Histomorphometry was used to quantify the area of new bone within the defect boundaries of the H&E stained sections (Fig. 5B). In agreement with the microCT results, the 64-star-PLL-pDual scaffold facilitated the highest area of new bone formation ($1.4 \times 10^6 \pm 4.6 \times 10^5$ μm^2), which was significantly increased over the 64-star-PLL-(no gene) scaffold ($8.1 \times 10^5 \pm 1.4 \times 10^5$ μm^2, $p < 0.01$), the 32-star-PLL-(no gene) scaffold ($7.6 \times 10^5 \pm 2.8 \times 10^5$ μm^2, $p < 0.01$) and the scaffold alone ($3.7 \times 10^5 \pm 7.5 \times 10^4$ μm^2, $p < 0.0001$). The 32-star-PLL-pDual group ($1.1 \times 10^6 \pm 3.5 \times 10^5$ μm^2) also resulted in significantly higher

new bone area compared to the scaffold alone ($p < 0.001$). In addition, a trend towards increased new bone volume was observed in both the 32-star-PLL-(no gene) scaffold & 64-star-PLL-(no gene) scaffold groups compared to the scaffold alone group, however this failed to reach significance.

High magnification images taken of each defect (Fig. 6(A–E)) using both H&E staining (i & ii) & Masson's Trichrome (MT) staining (iii & iv) further support the above claims. The scaffold alone group (Fig. 6A) demonstrated areas of high cell infiltration towards the periphery of the construct. Some positive staining for osteoid and new bone was present thereby highlighting the potential of the collagen-HA scaffold to function as a 3D template for tissue repair. However, this group was poorly integrated with the host at this early timepoint of 4 weeks, with clear boundaries between the scaffold/host tissue visible. Both the 32-star-PLL-pDual scaffold (Fig. 6C) and the 64-star-PLL-pDual scaffold (Fig. 6E) contained extensive mineralized osteoid. Notably, the 64-star-PLL-pDual scaffold contained extensive areas of new bone, resembling early stage woven bone. Histologically, increased new bone was evident in the 64-star-PLL-pDual group compared to the 32-star-PLL-pDual group. The 32-star-PLL-(no gene) scaffold (Fig. 6B) and the 64-star-PLL-(no gene) scaffold (Fig. 6D) groups contained evidence of osteoid and new bone which appeared enhanced over the scaffold alone group. Overall, bone tissue repair
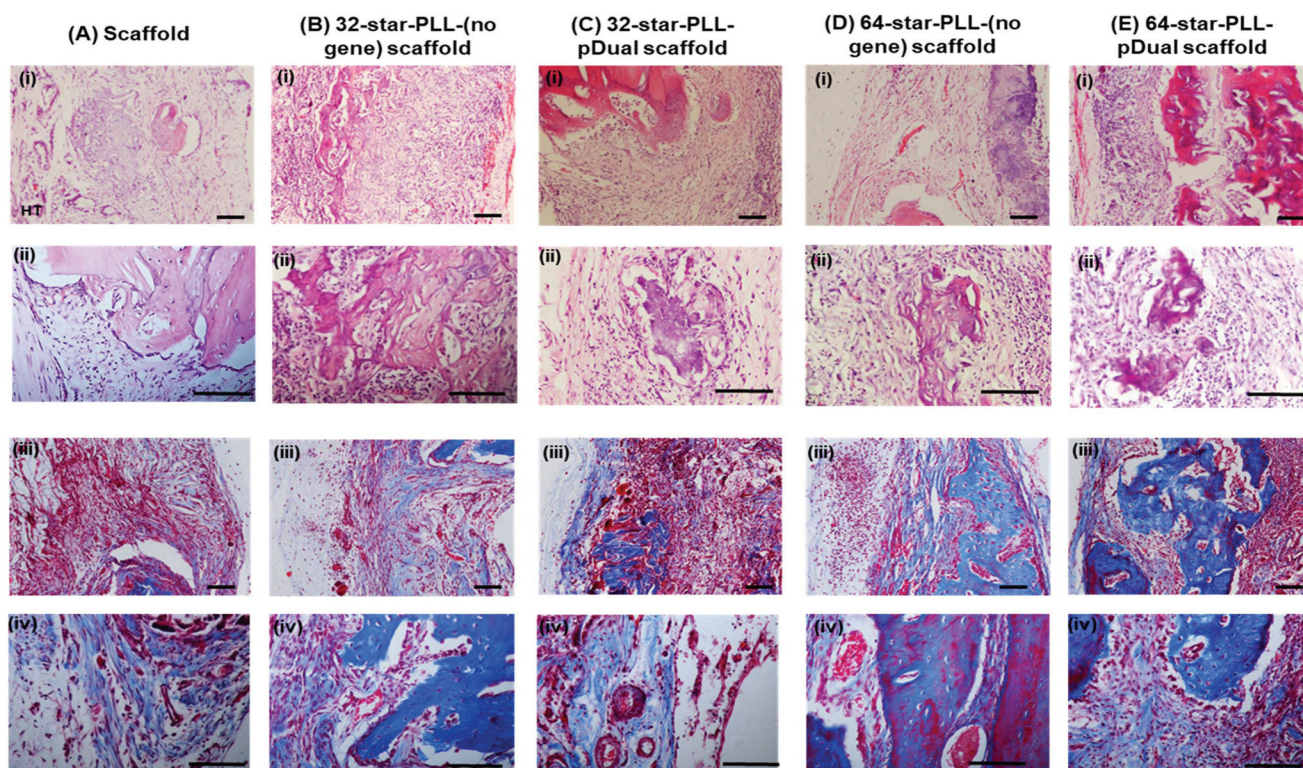

Fig. 6 Tissue appraisal using H&E and Masson's Trichrome staining. Representative high resolution (i & ii) H&E and (iii & iv) MT stained images of tissue present in a critical defect of male Wistar rats four weeks post treatment with various gene activated collagen-HA scaffolds (A–E). Groups assessed included (A) scaffold, (B) 32-star-PLL-(no gene) scaffold, (C) 32-star-PLL-pDual scaffold, (D) 64-star-PLL-(no gene) scaffold and (E) 64-star-PLL-pDual scaffold. Scale bar = 100 μm.

appeared more advanced in the 32-star-PLL-pDual and 64-star-PLL-pDual groups compared to their respective scaffold alone groups.

Discussion

Modern tissue engineering approaches increasingly use bioactive molecules to accelerate tissue regeneration. While therapeutic growth factors are commonly used as bioactive cues, the large, supraphysiological doses required to induce a healing response *in vivo* have been associated with complications such as the uncontrolled formation of ectopic tissue.[43] In this study we describe a potentially safer, alternative approach for TE by harnessing gene therapy and biomaterials science approaches to confer enhanced spatiotemporal control of growth factor production within a defect site. Due to the difficulty of transfecting MSCs,[44] there is a critical need for novel gene delivery vectors which are both biocompatible and capable of efficiently transfecting MSCs *in vivo* from 3D constructs. The accelerated bone repair observed in this study is achieved *via* the *in situ* transfection of autologous host cells within an implanted collagen based scaffold by a novel class of non-viral vector, star-PLLs. We have previously optimized these star-PLL vectors for TE applications both *in vitro*[45] and *in vivo*.[1] Herein, we demonstrate their therapeutic potential for the first time. A star-PLL with a high-arm density containing 64-poly(L-lysine) arms could successfully deliver a dual therapeutic cargo of pBMP-2 and pVEGF on collagen-based scaffolds *in vitro*. This gene-loaded scaffold induced enhanced MSC-mediated osteogenesis compared to single delivery of either pBMP-2 or pVEGF alone *in vitro*. This dual formulation approach exploits the synergistic effect of osteogenic–angiogenic coupling between pBMP-2 and pVEGF[20] allowing for an overall lower dose of each plasmid to be delivered compared to delivery of a single plasmid. The osteogenic potential of the gene activated scaffold was further increased when the macromolecular composition of the scaffold was varied to contain a ceramic hydroxyapatite component. *In vivo*, we highlight the translational potential of a 64-star-PLL-pDual collagen-HA scaffold which can facilitate the rapid regeneration of bone tissue within a critical sized rodent calvarial defect at the early timepoint of just 4 weeks. Overall, this study describes a cell-free, biomimetic gene activated scaffold incorporating star-polypeptides and a pDual therapeutic cargo which can induce accelerated bone formation *in vivo*.

The TE field is increasingly moving towards the delivery of multiple growth factors in tandem to better recapitulate the regenerative process.[46] Increasingly within the literature, there are reports of the dual delivery of either pDNA or growth factors to enhance bone tissue repair using combinations such as BMP-2 & VEGF,[20,21,29,40] BMP-2 & BMP-7,[47] BMP-4 & VEGF[17,48] and VEGF & PDGF.[49,50] In agreement with this, we report that the 64-star-PLL-pDual collagen-CS scaffold (pBMP-2 + pVEGF) resulted in a higher level of calcium deposition than that of the single delivery of pBMP-2 or pVEGF as

well as a scaffold alone *in vitro*. The 5 µg pDNA dose which was used to form each gene activated construct *in vitro* is similar to that previously used *in vivo* for bone repair within our group (4 µg).[29] This dose is, however, considerably lower than that which is often used for gene activated scaffolds within the literature which range from 12 µg–200 µg.[51–53] It has been reported that the mixing of two plasmids together prior to nanomedicine self-assembly results in the formation of dual loaded complexes, with a resultant increase in the number of cells co-expressing both plasmids.[54] Importantly, this pDual loaded formulation (2.5 µg pBMP-2 + 2.5 µg pVEGF) contained half the pDNA dose of each individual plasmid compared to that of individual gene formulations (5 µg pBMP-2 or 5 µg pVEGF). This highlights the potent synergism of the concurrent delivery of pBMP-2 & pVEGF, commonly referred to as the osteogenic–angiogenic coupling effect.[17] The 64-star-PLL vector likely possesses a higher loading capacity than the 32-star-PLL which allows it to better condense pDNA into a polyplex thereby acting as a more efficient vector. This is likely due to the higher density of shorter poly(L-lysine) arms on the 64-star-PLL (64 arms, 5 subunits long each) compared with the 32-star-PLL (32 arms, 40 subunits long each) which permits more efficient pDNA compaction.[31]

Upon application of the 64-star-PLL-pDual formulation to multiple composite scaffold types *in vitro*, we observed enhanced MSC mediated osteogenesis compared to the respective scaffolds for each of collagen ($p < 0.5$), collagen-HyA ($p < 0.5$), collagen-HA ($p < 0.5$) and collagen-nHA ($p < 0.001$) scaffolds. Notably, the versatility of the 64-star-PLL vector and its efficiency for pDNA delivery to MSCs allowed the functionalization of all composite scaffold types for enhanced MSC osteogenesis. This finding further highlights the potential of the star-PLL-pDual formulation for bone tissue engineering as it could induce significant osteogenesis on a scaffold with little intrinsic osteogenic potential such as the collagen-HyA scaffold. As the range of scaffolds can be applied for multiple different tissue engineering defects, it also suggests that star-PLLs are promising vectors for tissue repair in a multitude of applications.

The highest level of MSC mediated calcium deposition was found using the gene activated collagen-HA scaffold. This is perhaps unsurprising, as the significant potential of this collagen-HA scaffold for bone repair has been highlighted in a recent report of the healing of a mandibular bone cyst in a thoroughbred filly as early as 3 months[8] as well as in multiple small animal studies including rabbits[55] and rodents.[4] To isolate the inherent osteogenic effects each scaffold may or may not possess, and thus truly assess which macromolecular composition best supports gene mediated osteogenesis, each determined calcium value was normalized to that achieved by its respective scaffold alone cultured in OM. Overall, these findings highlighted scaffolds which contain a ceramic macromolecular component (collagen-nHA and collagen-HA) as most suited to supporting star-PLL-pDual mediated MSC osteogenesis. This observation suggests that the star-polymer structure could be tailored in terms of its amino acid compo-

sition, arm number & arm length to achieve maximum therapeutic potential with a specific scaffold composite.

An interesting observation was a trend towards increased levels of calcium deposited per scaffold when loaded with the 64-star-PLL-(no gene) formulation compared to the scaffold alone groups. This suggests an intrinsic osteogenic potential of the 64-star-PLL vector. Within the literature there are multiple reports which suggest that L-lysine amino acid supplementation can induce an enhanced osteogenic response *via* the direct stimulation of osteoblasts.[56–60] Interestingly, this effect was star-polypeptide dependent as we did not find a significant increase in osteogenesis when either of the star-polypeptide architectural components *i.e.* linear poly(L-lysine) or a poly(propyleneimine) dendrimer were used to treat MSCs. This rather serendipitous finding suggests that in the search for an ideal vector for TE applications, the effects of the chemical structure itself should be taken into consideration as a potential bioactive component of the formulation, independent of its transfection capability.[61]

We next assessed the ability of these optimised star-PLL-pDual gene activated scaffolds to accelerate the healing of a critical sized rodent calvarial defect after just four weeks. The 64-star-PLL-pDual scaffold exhibited the highest new bone volume within the defect at 4 weeks compared to all other groups. Of note, the levels of new bone volume achieved by this group was 6-fold increased over the scaffold alone group, 4-fold increased over the 32-star-PLL-(no gene) scaffold group and 2-fold increased over the 64-star-PLL-(no gene) group. Furthermore, in support of our previous comparative studies on both the 32- & 64-star-PLL vectors *in vitro*,[1] the 64-star-PLL-pDual scaffold group resulted in a higher new bone volume compared to the 32-star-PLL-pDual group. Impressively, the quantitative microCT values obtained here using this 64-star-PLL-pDual scaffold group *i.e.* a gene-based approach, are in line with those obtained by Patel *et al.* in a similar model following the dual delivery of the growth factor proteins BMP-2 (2 µg) & VEGF (12 µg) directly at 4 weeks.[20]

The superiority of the 64-star-PLL-pDual group over that of the control groups was further confirmed using both qualitative and quantitative histological assessment. The 64-star-PLL-pDual scaffolds were highly cellularised and appeared primarily occupied by new bone or highly mineralized osteoid. Quantitatively, the 64-star-PLL-pDual facilitated a 3.8 fold increased in new bone area compared to the scaffold alone group, a 1.8-fold increase compared to the 32-star-PLL-(no gene) scaffold group and a 1.7-fold increase compared to the 64-star-PLL-(no gene) scaffold group. This accelerated level of new bone formation was observed at just four weeks post implantation, a very short time frame for the healing of a critical sizes bone defect.[62]

We attribute the success of this 64-star-PLL-pDual group to two components, namely the delivered pDual cargo and the highly efficient 64-star-PLL vector. Both the potent osteogenic potential of BMP-2[63] and the angiogenic/osteogenic potential of VEGF[16] are well established individually. However, their dual delivery is somewhat more contested, with reports that

combinatorial therapy can function to harness the potent osteogenic–angiogenic coupling necessary to form vascularized, mature bone.[17,40] While others have suggested that the dual delivery of BMP-2 and VEGF does not confer a beneficial increase in bone healing compared to BMP-2 alone.[64] That said, based on previous *in vitro* work,[31] the level of VEGF protein produced within each gene activated scaffold will likely be much lower than that of BMP-2 protein. This may further contribute to the success of the system, as it has been reported within the literature that the synergistic interplay between VEGF and BMP-2 in mediating osteogenesis is dependent on the ratio of these factors, with a lower VEGF : BMP ratio demonstrating enhanced bone repair.[65]

The regenerative capacity is likely further enhanced by the 64-star-PLL vectors' ability to efficiently condense the pDual cargo, prevent its degradation *in vivo*, mediate nanomedicine retention within the scaffold and facilitate the 3D transfection of infiltrating MSCs as we have previously described.[1,31] Indeed, multiple 64-star-PLL-pDual specimens displayed an advanced level of bone healing with partial defect bridging, the clear infiltration of autologous host cells and only a small area of unmineralised osteoid remaining within the defect center. This observation suggests that healing occurs from the defect boundaries inwards, a finding supported by others whom suggested that within a critical defect, osteoprogenitor cells potentially migrate from the dura mater into the scaffold architecture.[66] Overall, these two attributes function to create a highly osteoinductive gene activated construct with significant potential for the healing of critical sized defects. The bone repair observed in this study compares favorably with gene activated scaffolds created in our lab using vectors such as chitosan[40] and nanophase-hydroxyapatite.[29] Furthermore, the results presented here are favorable when it is considered that higher pDNA doses in the region of 50 µg pDNA (pPDGF)/ scaffold have been used by others to achieve ~40% BV/TV.[51]

The innate osteogenic potential of the star-PLL vector which we observed in 3D studies *in vitro* translated only to a minor extent *in vivo*. While there are reports of the use of lysine to stimulate osteogenesis both *in vitro*[59,67,68] and *in vivo*,[58] they are often used at much higher concentrations (*e.g.* 47 mg kg⁻¹).[56] The µg quantities utilised in this study within each scaffold failed to provide an adequate osteogenic stimulus *in vivo*. Nonetheless, a trend towards both enhanced new bone volume and new bone area is evident for both star-PLL vectors over that of the scaffold alone group. The presence of new bone deposits in some specimens from both groups thereby suggesting the architecture likely contributes some intrinsic, albeit minor osteogenic potential to the scaffolds.

Currently, INFUSE® bone graft (Medtronic) is the most widely used TE product for bone repair clinically available. It consists of a collagen sponge soak loaded with rhBMP-2 for the regeneration of bone tissue in lumbar spinal fusion procedures. While accepted clinically, this formulation exhibits poor growth factor release kinetics causing a supraphysiological level of BMP-2 protein at the defect site. This has been linked to a number of side effects such as ectopic bone for-

mation, cytotoxicity, renal complications and a potential increased malignancy risk.[23] In contrast, the 64 star-PLL-pDual gene activated scaffold described herein is capable of producing transient, localized and temporally sustained expression of BMP-2 and VEGF proteins at the bone defect site. This gene-activated scaffold necessitates a smaller delivered dose of therapeutic cargo leading to more appropriate physiological concentrations.[69] The ability of the scaffold to function as a nanomedicine depot,[1] and thus mediate the local transfection of host cells should further function to mitigate off target side effects as both BMPs and VEGF are not specific to bone tissue.[70,71] From a biomaterial viewpoint, the HA component of the scaffold can further function to attract and sequester endogenous BMP proteins thereby further increasing the osteogenic stimulus within the defect.[72] Finally, both the pBMP-2/pVEGF genetic cargo and the star-PLL vectors are relatively inexpensive to produce on a large scale and possess an ease of handling for the end user which is not possible with the more sensitive rhBMP-2 molecules. Overall, the use of a novel, bio-inspired star-PLL vector, which is biocompatible, possesses a high cargo loading capacity and is relatively straightforward to formulate with a pDNA cargo has enabled the formation of an efficient platform which could potentially be applied for multiple tissue engineering applications.

Conclusion

Herein, we illustrate for the first time that a novel class of biomaterials in the form of star-PLLs are capable of successfully delivering a therapeutic pDNA cargo from a collagen based scaffold *in vivo* with demonstrated ability to regenerate bone tissue. *In vitro*, we demonstrate that the dual delivery of pBMP-2 and pVEGF using the 64-star-PLL vector can be used to induce MSC-mediated osteogenesis on a range of collagen-based scaffolds with different macromolecular compositions. This dual therapy can harness the potent, synergistic osteogenic–angiogenic coupling effect of its two plasmid components to facilitate enhanced MSC mediated osteogenesis at a lower pDNA dose compared to individual delivery of pBMP-2 or pVEGF. *In vivo*, we demonstrate that this optimized 64-star-PLL-pDual collagen-HA scaffold can accelerate new bone formation within a critical sized rodent calvarial defect. At the very early timepoint of just 4 weeks post implantation, the 64-star-PLL-pDual gene activated scaffold caused a 6-fold increase in new bone formation compared to a scaffold alone and a 4-fold increase compared to a 32-star-PLL-pDual gene activated scaffold. Finally, we make the interesting observation that the star-PLL vector possesses a mild osteogenic profile itself, when delivered without a gene cargo. Overall, we highlight the potential of the star-shaped polypeptide vector as a versatile, biocompatible biomaterial with high cargo loading capacity which can deliver multiple therapeutic transgenes *in vivo* from a collagen-HA scaffold and facilitate accelerated bone tissue regeneration.

Conflicts of interest

There are no conflicts to declare.

Acknowledgements

References

1 D. P. Walsh, R. M. Raftery, I. M. Castaño, R. Murphy, B. Cavanagh, A. Heise, *et al.*, Transfection of autologous host cells in vivo using gene activated collagen scaffolds incorporating star-polypeptides, *J. Controlled Release*, 2019, **304**, 191–203.

2 C. M. Murphy, M. G. Haugh and F. J. O'Brien, The effect of mean pore size on cell attachment, proliferation and migration in collagen-glycosaminoglycan scaffolds for bone tissue engineering, *Biomaterials*, 2010, **31**(3), 461–466.

3 A. Matsiko, T. J. Levingstone, F. J. O'Brien and J. P. Gleeson, Addition of hyaluronic acid improves cellular infiltration and promotes early-stage chondrogenesis in a collagen-based scaffold for cartilage tissue engineering, *J. Mech. Behav. Biomed. Mater.*, 2012, **11**, 41–52.

4 J. P. Gleeson, N. A. Plunkett and F. J. O'Brien, Addition of hydroxyapatite improves stiffness, interconnectivity and osteogenic potential of a highly porous collagen-based scaffold for bone tissue regeneration, *Eur. Cells Mater.*, 2010, **20**, 218–230.

5 G. M. Cunniffe, G. R. Dickson, S. Partap, K. T. Stanton and F. J. O'Brien, Development and characterisation of a collagen nano-hydroxyapatite composite scaffold for bone tissue engineering, *J. Mater. Sci.: Mater. Med.*, 2010, **21**(8), 2293–2298.

6 F. G. Lyons, A. A. Al-Munajjed, S. M. Kieran, M. E. Toner, C. M. Murphy, G. P. Duffy, *et al.*, The healing of bony defects by cell-free collagen-based scaffolds compared to stem cell-seeded tissue engineered constructs, *Biomaterials*, 2010, **31**(35), 9232–9243.

7 T. J. Levingstone, A. Ramesh, R. T. Brady, P. A. J. Brama, C. Kearney, J. P. Gleeson, *et al.*, Cell-free multi-layered collagen-based scaffolds demonstrate layer specific regeneration of functional osteochondral tissue in caprine joints, *Biomaterials*, 2016, **87**(Supplement C), 69–81.

8 F. David, T. J. Levingstone, W. Schneeweiss, M. de Swarte, H. Jahns, J. P. Gleeson, *et al.*, Enhanced bone healing using collagen-hydroxyapatite scaffold implantation in the treatment of a large multiloculated mandibular aneurysmal

bone cyst in a thoroughbred filly, *J. Tissue Eng. Regener. Med.*, 2015, 1193–1199.

9 P. Diaz-Rodriguez, M. Sánchez and M. Landin, Drug-Loaded Biomimetic Ceramics for Tissue Engineering, *Pharmaceutics*, 2018, **10**(4), 272.

10 R. Subbiah, M. P. Hwang, S. Y. Van, S. H. Do, H. Park, K. Lee, *et al.*, Osteogenic/angiogenic dual growth factor delivery microcapsules for regeneration of vascularized bone tissue, *Adv. Healthcare Mater.*, 2015, **4**(13), 1982–1992.

11 Y. Zhang, L. Wei, C. Wu and R. J. Miron, Periodontal regeneration using strontium-loaded mesoporous bioactive glass scaffolds in osteoporotic rats, *PLoS One*, 2014, **9**(8), e104527.

12 S. Verrier, M. Alini, E. Alsberg, S. R. Buchman, D. Kelly, M. W. Laschke, *et al.*, Tissue engineering and regenerative approaches to improving the healing of large bone defects, *Eur. Cells Mater.*, 2016, **32**, 87–110.

13 T. N. Vo, F. K. Kasper and A. G. Mikos, Strategies for controlled delivery of growth factors and cells for bone regeneration, *Adv. Drug Delivery Rev.*, 2012, **64**(12), 1292–1309.

14 A. Valentin-Opran, J. Wozney, C. Csimma, L. Lilly and G. E. Riedel, Clinical evaluation of recombinant human bone morphogenetic protein-2, *Clin. Orthop. Relat. Res.*, 2002, (395), 110–120.

15 R. A. D. Carano and E. H. Filvaroff, Angiogenesis and bone repair, *Drug Discovery Today*, 2003, **8**(21), 980–989.

16 J. Street, M. Bao, L. deGuzman, S. Bunting, F. V. Peale Jr., N. Ferrara, *et al.*, Vascular endothelial growth factor stimulates bone repair by promoting angiogenesis and bone turnover, *Proc. Natl. Acad. Sci. U. S. A.*, 2002, **99**(15), 9656–9661.

17 H. Peng, V. Wright, A. Usas, B. Gearhart, H. C. Shen, J. Cummins, *et al.*, Synergistic enhancement of bone formation and healing by stem cell-expressed VEGF and bone morphogenetic protein-4, *J. Clin. Invest.*, 2002, **110**(6), 751–759.

18 D. E. Ingber, V. C. Mow, D. Butler, L. Niklason, J. Huard, J. Mao, *et al.*, Tissue engineering and developmental biology: going biomimetic, *Tissue Eng.*, 2006, **12**(12), 3265–3283.

19 D. H. R. Kempen, L. Lu, A. Heijink, T. E. Hefferan, L. B. Creemers, A. Maran, *et al.*, Effect of local sequential VEGF and BMP-2 delivery on ectopic and orthotopic bone regeneration, *Biomaterials*, 2009, **30**(14), 2816–2825.

20 Z. S. Patel, S. Young, Y. Tabata, J. A. Jansen, M. E. K. Wong and A. G. Mikos, Dual delivery of an angiogenic and an osteogenic growth factor for bone regeneration in a critical size defect model, *Bone*, 2008, **43**(5), 931–940.

21 R. M. Raftery, D. P. Walsh, L. Blokpoel Ferreras, I. Mencía Castaño, G. Chen, M. LeMoine, *et al.*, Highly versatile cell-penetrating peptide loaded scaffold for efficient and localised gene delivery to multiple cell types: From development to application in tissue engineering, *Biomaterials*, 2019, **216**, 119277.

22 D. P. Walsh, R. M. Raftery, G. Chen, A. Heise, F. J. O'Brien and S. A. Cryan, Rapid healing of a critical-sized bone

23 E. J. Carragee, E. L. Hurwitz and B. K. Weiner, A critical review of recombinant human bone morphogenetic protein-2 trials in spinal surgery: emerging safety concerns and lessons learned, *Spine J.*, 2011, **11**(6), 471–491.

24 R. M. Raftery, D. P. Walsh, I. M. Castano, A. Heise, G. P. Duffy, S. A. Cryan, *et al.*, Delivering Nucleic-Acid Based Nanomedicines on Biomaterial Scaffolds for Orthopedic Tissue Repair: Challenges, Progress and Future Perspectives, *Adv. Mater.*, 2016, **28**(27), 5447–5469.

25 D. P. Walsh, A. Heise, F. J. O'Brien and S. A. Cryan, An efficient, non-viral dendritic vector for gene delivery in tissue engineering, *Gene Ther.*, 2017, **24**, 681.

26 J. Fang, Y. Y. Zhu, E. Smiley, J. Bonadio, J. P. Rouleau, S. A. Goldstein, *et al.*, Stimulation of new bone formation by direct transfer of osteogenic plasmid genes, *Proc. Natl. Acad. Sci. U. S. A.*, 1996, **93**(12), 5753–5758.

27 J. Bonadio, E. Smiley, P. Patil and S. Goldstein, Localized, direct plasmid gene delivery in vivo: prolonged therapy results in reproducible tissue regeneration, *Nat. Med.*, 1999, **5**(7), 753–759.

28 W. Godbey, K. K. Wu and A. G. Mikos, Poly (ethylenimine)-mediated gene delivery affects endothelial cell function and viability, *Biomaterials*, 2001, **22**(5), 471–480.

29 C. M. Curtin, E. G. Tierney, K. McSorley, S. A. Cryan, G. P. Duffy and F. J. O'Brien, Combinatorial gene therapy accelerates bone regeneration: non-viral dual delivery of VEGF and BMP2 in a collagen-nanohydroxyapatite scaffold, *Adv. Healthcare Mater.*, 2015, **4**(2), 223–227.

30 J. M. Ren, T. G. McKenzie, Q. Fu, E. H. H. Wong, J. Xu, Z. An, *et al.*, Star Polymers, *Chem. Rev.*, 2016, **116**(12), 6743–6836.

31 D. P. Walsh, R. D. Murphy, A. Panarella, R. M. Raftery, B. Cavanagh, J. C. Simpson, *et al.*, Bioinspired Star-Shaped Poly(l-lysine) Polypeptides: Efficient Polymeric Nanocarriers for the Delivery of DNA to Mesenchymal Stem Cells, *Mol. Pharm.*, 2018, **15**(5), 1878–1891.

32 M. Byrne, D. Victory, A. Hibbitts, M. Lanigan, A. Heise and S.-A. Cryan, Molecular weight and architectural dependence of well-defined star-shaped poly(lysine) as a gene delivery vector, *Biomater. Sci.*, 2013, **1**(12), 1223–1234.

33 F. J. O'Brien, B. A. Harley, I. V. Yannas and L. Gibson, Influence of freezing rate on pore structure in freeze-dried collagen-GAG scaffolds, *Biomaterials*, 2004, **25**(6), 1077–1086.

34 R. M. Raftery, E. G. Tierney, C. M. Curtin, S. A. Cryan and F. J. O'Brien, Development of a gene-activated scaffold platform for tissue engineering applications using chitosan-pDNA nanoparticles on collagen-based scaffolds, *J. Controlled Release*, 2015, **210**, 84–94.

35 I. M. Castano, C. M. Curtin, G. Shaw, J. M. Murphy, G. P. Duffy and F. J. O'Brien, A novel collagen-nanohydroxyapatite microRNA-activated scaffold for tissue engineering applications capable of efficient delivery of both miR-

defect using a collagen-hydroxyapatite scaffold to facilitate low dose, combinatorial growth factor delivery, *J. Tissue Eng. Regener. Med.*, 2019, (10), 1843–1853.

mimics and antagomiRs to human mesenchymal stem cells, *J. Controlled Release*, 2015, **200**, 42–51.

36 M. G. Haugh, C. M. Murphy, R. C. McKiernan, C. Altenbuchner and F. J. O'Brien, Crosslinking and mechanical properties significantly influence cell attachment, proliferation, and migration within collagen glycosaminoglycan scaffolds, *Tissue Eng., Part A*, 2011, **17**(9–10), 1201–1208.

37 P. F. O'Loughlin, S. Morr, L. Bogunovic, A. D. Kim, B. Park and J. M. Lane, Selection and development of preclinical models in fracture-healing research, *J. Bone Jt. Surg., Am. Vol.*, 2008, **90**(Suppl 1), 79–84.

38 P. P. Spicer, J. D. Kretlow, S. Young, J. A. Jansen, F. K. Kasper and A. G. Mikos, Evaluation of bone regeneration using the rat critical size calvarial defect, *Nat. Protocols*, 2012, **7**(10), 1918–1929.

39 M. Alhag, E. Farrell, M. Toner, T. C. Lee, F. J. O'Brien and N. Claffey, Evaluation of the ability of collagen-glycosaminoglycan scaffolds with or without mesenchymal stem cells to heal bone defects in Wistar rats, *Oral Maxillofac. Surg.*, 2012, **16**(1), 47–55.

40 R. M. Raftery, I. Mencia Castaño, G. Chen, B. Cavanagh, B. Quinn, C. M. Curtin, *et al.*, Translating the role of osteogenic-angiogenic coupling in bone formation: Highly efficient chitosan-pDNA activated scaffolds can accelerate bone regeneration in critical-sized bone defects, *Biomaterials*, 2017, **149**, 116–127.

41 E. Quinlan, A. López-Noriega, E. Thompson, H. M. Kelly, S. A. Cryan and F. J. O'Brien, Development of collagen–hydroxyapatite scaffolds incorporating PLGA and alginate microparticles for the controlled delivery of rhBMP-2 for bone tissue engineering, *J. Controlled Release*, 2015, **198**, 71–79.

42 J. Schindelin, I. Arganda-Carreras, E. Frise, V. Kaynig, M. Longair, T. Pietzsch, *et al.*, Fiji: an open-source platform for biological-image analysis, *Nat. Methods*, 2012, **9**(7), 676–682.

43 M. Miyazaki, H. Tsumura, J. C. Wang and A. Alanay, An update on bone substitutes for spinal fusion, *Eur. Spine J.*, 2009, **18**(6), 783–799.

44 A. Hamm, N. Krott, I. Breibach, R. Blindt and A. K. Bosserhoff, Efficient transfection method for primary cells, *Tissue Eng.*, 2002, **8**(2), 235–245.

45 D. P. Walsh, R. D. Murphy, A. Panarella, R. M. Raftery, B. Cavanagh, J. C. Simpson, *et al.*, Bioinspired Star-Shaped Poly(L-Lysine) Polypeptides; Efficient Polymeric Nanocarriers for the Delivery of DNA to Mesenchymal Stem Cells, *Mol. Pharm.*, 2018, 1878–1891.

46 F.-M. Chen, M. Zhang and Z.-F. Wu, Toward delivery of multiple growth factors in tissue engineering, *Biomaterials*, 2010, **31**(24), 6279–6308.

47 J. T. Koh, Z. Zhao, Z. Wang, I. S. Lewis, P. H. Krebsbach and R. T. Franceschi, Combinatorial gene therapy with BMP2/7 enhances cranial bone regeneration, *J. Dent. Res.*, 2008, **87**(9), 845–849.

48 G. Li, K. Corsi-Payne, B. Zheng, A. Usas, H. Peng and J. Huard, The dose of growth factors influences the synergistic effect of vascular endothelial growth factor on bone morphogenetic protein 4-induced ectopic bone formation, *Tissue Eng., Part A*, 2009, **15**(8), 2123–2133.

49 S. D'Mello, S. Elangovan, L. Hong, R. D. Ross, D. R. Sumner and A. K. Salem, A Pilot Study Evaluating Combinatorial and Simultaneous Delivery of Polyethylenimine-Plasmid DNA Complexes Encoding for VEGF and PDGF for Bone Regeneration in Calvarial Bone Defects, *Curr. Pharm. Biotechnol.*, 2015, **16**(7), 655–660.

50 B. De la Riva, E. Sánchez, A. Hernández, R. Reyes, F. Tamimi, E. López-Cabarcos, *et al.*, Local controlled release of VEGF and PDGF from a combined brushite–chitosan system enhances bone regeneration, *J. Controlled Release*, 2010, **143**(1), 45–52.

51 S. Elangovan, S. R. D'Mello, L. Hong, R. D. Ross, C. Allamargot, D. V. Dawson, *et al.*, The Enhancement of Bone Regeneration by Gene Activated Matrix Encoding for Platelet Derived Growth Factor, *Biomaterials*, 2014, **35**(2), 737–747.

52 M. Endo, S. Kuroda, H. Kondo, Y. Maruoka, K. Ohya and S. Kasugai, Bone regeneration by modified gene-activated matrix: effectiveness in segmental tibial defects in rats, *Tissue Eng.*, 2006, **12**(3), 489–497.

53 Y. C. Huang, K. Riddle, K. G. Rice and D. J. Mooney, Long-term in vivo gene expression via delivery of PEI-DNA condensates from porous polymer scaffolds, *Hum. Gene Ther.*, 2005, **16**(5), 609–617.

54 N. S. Bhise, R. B. Shmueli, J. Gonzalez and J. J. Green, A novel assay for quantifying the number of plasmids encapsulated by polymer nanoparticles, *Small*, 2012, **8**(3), 367–373.

55 F. G. Lyons, J. P. Gleeson, S. Partap, K. Coghlan and F. J. O'Brien, Novel microhydroxyapatite particles in a collagen scaffold: a bioactive bone void filler?, *Clin. Orthop. Relat. Res.*, 2014, **472**(4), 1318–1328.

56 S. Sinha and S. C. Goel, Effect of amino acids lysine and arginine on fracture healing in rabbits: A radiological and histomorphological analysis, *Indian J. Orthop.*, 2009, **43**(4), 328–334.

57 M. Fini, R. Giardino, N. Nicoli Aldini, L. Martini, M. Rocca, F. Bertoni, *et al.*, Role of lactose, arginine and lysine combination in fracture healing (an experimental study), *Ann. Ital. Chir.*, 1996, **67**(1), 77–82.

58 M. Fini, P. Torricelli, G. Giavaresi, A. Carpi, A. Nicolini and R. Giardino, Effect of L-lysine and L-arginine on primary osteoblast cultures from normal and osteopenic rats, *Biomed. Pharmacother.*, 2001, **55**(4), 213–220.

59 P. Torricelli, M. Fini, G. Giavaresi, R. Giardino, S. Gnudi, A. Nicolini, *et al.*, L-Arginine and L-Lysine stimulation on cultured human osteoblasts, *Biomed. Pharmacother.*, 2002, **56**(10), 492–497.

60 *Osteogenic influence of lysine in porous hydroxyapatite scaffold*, ed. Tsuji N., Yoshikawa M., Shimomura Y., Yabuuchi T. and Hayashi H., Ohgushi H., 2008.

61 T. Gonzalez-Fernandez, B. N. Sathy, C. Hobbs, G. M. Cunniffe, H. O. McCarthy, N. J. Dunne, *et al.*,

Mesenchymal stem cell fate following non-viral gene transfection strongly depends on the choice of delivery vector, *Acta Biomater.*, 2017, **55**, 226–238.

62 P. Garcia, T. Histing, J. H. Holstein, M. Klein, M. W. Laschke, R. Matthys, *et al.*, Rodent animal models of delayed bone healing and non-union formation: a comprehensive review, *Eur. Cells Mater.*, 2013, **26**, 1–12, discussion -4.

63 A. Yamaguchi, T. Komori and T. Suda, Regulation of osteoblast differentiation mediated by bone morphogenetic proteins, hedgehogs, and Cbfa1, *Endocr. Rev.*, 2000, **21**(4), 393–411.

64 A. Hernandez, R. Reyes, E. Sanchez, M. Rodriguez-Evora, A. Delgado and C. Evora, In vivo osteogenic response to different ratios of BMP-2 and VEGF released from a biodegradable porous system, *J. Biomed. Mater. Res., Part A*, 2012, **100**(9), 2382–2391.

65 H. Peng, A. Usas, A. Olshanski, A. M. Ho, B. Gearhart, G. M. Cooper, *et al.*, VEGF improves, whereas sFlt1 inhibits, BMP2-induced bone formation and bone healing through modulation of angiogenesis, *J. Bone Miner. Res.*, 2005, **20**(11), 2017–2027.

66 B. Behr, M. Sorkin, M. Lehnhardt, A. Renda, M. T. Longaker and N. Quarto, A comparative analysis of the osteogenic effects of BMP-2, FGF-2, and VEGFA in a calvarial defect model, *Tissue Eng., Part A*, 2012, **18**(9–10), 1079–1086.

67 M. Yoshikawa, Y. Shimomura, H. Kakigi, N. Tsuji, T. Yabuuchi and H. Hayashi, Effect of L-lysine in culture medium on nodule formation by bone marrow cells, *J. Biomed. Sci. Eng.*, 2012, **05**(10), 587–592.

68 H. Y. Zhou, Y. Ohnuma, H. Takita, R. Fujisawa, M. Mizuno and Y. Kuboki, Effects of a bone lysine-rich 18 kDa protein on osteoblast-like MC3T3-E1 cells, *Biochem. Biophys. Res. Commun.*, 1992, **186**(3), 1288–1293.

69 K. A. Blackwood, N. Bock, T. R. Dargaville and M. Ann Woodruff, Scaffolds for Growth Factor Delivery as Applied to Bone Tissue Engineering, *Int. J. Polym. Sci.*, 2012, **2012**, 25.

70 N. Ferrara, H. P. Gerber and J. LeCouter, The biology of VEGF and its receptors, *Nat. Med.*, 2003, **9**(6), 669–676.

71 D. Chen, M. Zhao and G. R. Mundy, Bone morphogenetic proteins, *Growth Factors*, 2004, **22**(4), 233–241.

72 T. Boix, J. Gomez-Morales, J. Torrent-Burgues, A. Monfort, P. Puigdomenech and R. Rodriguez-Clemente, Adsorption of recombinant human bone morphogenetic protein rhBMP-2 m onto hydroxyapatite, *J. Inorg. Biochem.*, 2005, **99**(5), 1043–1050.